

Figure 1: Sketch of the model.

## Protostellar jets and magnetic diffusion

Miljenko Čemeljić<sup>1</sup> and Christian Fendt<sup>1,2</sup>

<sup>1</sup>Astrophysikalisches Institut Potsdam (Germany), <sup>2</sup>Universität Potsdam, Institut für Physik; email: cemeljic,cfendt@aip.de

### Abstract

We investigate the evolution of a disk wind into a collimated jet under the influence of magnetic diffusivity. Using the ZEUS-3D code in the axisymmetry option we solve the time-dependent resistive MHD equations for a model setup of a central star surrounded by an accretion disk. The disk is taken as a time-independent boundary condition for the mass flow rate and the magnetic flux distribution. We find that the diffusive jets propagate slower into the ambient medium, most probably due to the lower mass flow rate in axial direction. Close to the star we find that a quasi stationary state evolves after several hundreds (weak diffusion) or thousands (strong diffusion) of disk rotations. Magnetic diffusivity affects the protostellar jet structure de-collimating it. We explain these effects in the framework of the Lorentz force.

keywords: accretion, accretion disks – MHD – ISM: jets and outflows – stars: mass loss – stars: pre-main sequence

## 1 Magnetic jets from accretion disks

Astrophysical jets detected so far seem to be attached to objects where an accretion disk is indicated to be present. The similarities between jets from the different sources imply that the basic mechanism for jet formation should be the same.

What kind of mechanism turns the inflowing matter of the accretion disk into an outflow from the disk (or the star) is still not really known, although it seems to be clear that magnetic fields play a major role.

Our model is sketched in Figure 1. In order to model the time-dependent evolution of jet formation, we solve the set of resistive MHD equations,

$$\frac{\partial \rho}{\partial t} + \nabla \cdot (\rho \vec{v}) = 0 \quad (1)$$

$$\rho \left[ \frac{\partial \vec{u}}{\partial t} + (\vec{v} \cdot \nabla) \vec{v} \right] + \nabla(p + p_A) + \rho \nabla \Phi - \frac{\vec{j} \times \vec{B}}{c} = 0 \quad (2)$$

$$\frac{\partial \vec{B}}{\partial t} - \nabla \times \left( \vec{v} \times \vec{B} - \frac{4\pi}{c} \eta \vec{j} \right) = 0 \quad (3)$$

$$e = p/(\gamma - 1) \quad (4)$$

$$\nabla \cdot \vec{B} = 0 \quad (5)$$

$$\frac{4\pi}{c} \vec{j} = \nabla \times \vec{B} . \quad (6)$$

We apply a polytropic equation of state,  $p = K\rho^\gamma$  with a polytropic index  $\gamma = 5/3$ . We do not solve the energy equation but define the internal energy of the system with eq. (4). We may expect that the turbulence pattern in the disk may also enter the disk corona and the jet, and that the jet flow itself is subject to turbulent diffusion. The magnetic diffusivity is denoted by the variable  $\eta$ , and other have its usual meaning, with  $p_A \equiv p/\beta_T$  with  $\beta_T = \text{const.}$ , an Alfvénic turbulent pressure, added to the hydrostatic pressure  $p$ .

## 2 Results and discussion

The results of one reference set of global simulations with high resolution (numerical mesh of  $900 \times 200$  grid points, physical grid of  $(z \times r) = (280 \times 40)r_i$ ) are presented in Figure 2.

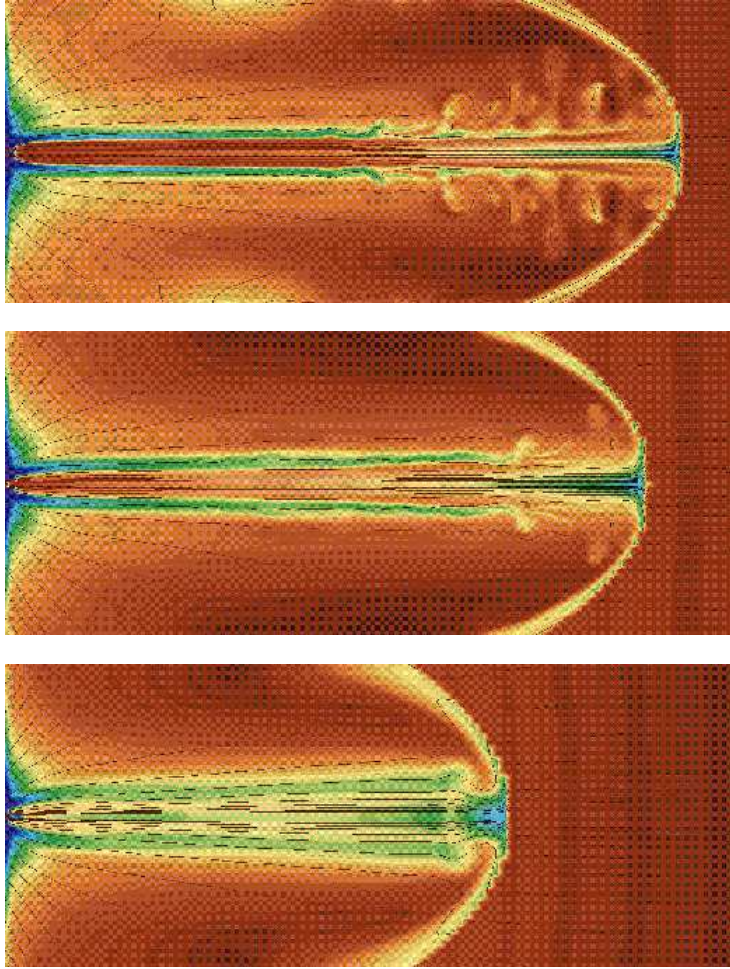


Figure 2: Global evolution of the jet on a grid of  $(z \times r) = (280 \times 40)r_i$  with a resolution of  $900 \times 200$  elements. Shown is the state of evolution after  $t=400$  rotations of the disk inner radius for different magnetic diffusivity,  $\eta=0, 0.01, 0.1$  for top, middle and bottom panel, respectively. Colors (blue to yellow in decreasing manner) indicate density. Lines denote twenty linearly spaced magnetic flux surfaces (or poloidal field lines). The figure demonstrates that the bow shock advances slower with increasing diffusivity.

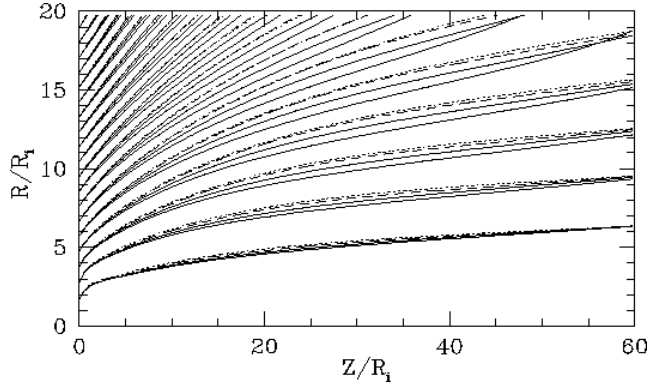


Figure 3: The evolution of the inner jet approaches the quasi-stationary state. Shown are poloidal magnetic field lines in the case of  $\eta = 0.1$  for different time steps,  $t = 250, 300, 350, 400$  (thick solid, thin solid, dashed and dotted lines, respectively). In these simulations beta plasma is half the value from the global simulations above, but this just changes the position of the Alfvén surface above the disk slightly. Grid size is  $280 \times 80$  elements for a physical size of  $(140 \times 40)r_i$ . The picture shows how the poloidal magnetic field lines diffuse outwards but approach a (quasi)-stationary state after 400 rotations (see the dashed and dotted lines almost coinciding).

In order to investigate only the gross behavior of the jet flow and not its structure in detail, we run another set of simulations with lower resolution (numerical mesh of  $280 \times 80$  grid points, physical grid of  $(z \times r) = (140 \times 40)r_i$ ) – see Figure 3.

In apparent contrast with the bow shock propagation from Figure 2 is the increase of the jet velocity with diffusivity (Figure 4, left panel).

Below the “critical  $\eta$ ” in our choice of parameters ( $\eta < 0.5$ ), the time of reaching the quasi-stationary state of the inner jet is approximately linearly dependent on  $\eta$  (Figure 4, right panel).

Interesting is to note that de-collimation of the poloidal magnetic field lines is not followed by the poloidal velocity vectors – see Figure 5.

The much faster computation of the low resolution simulations allowed us to follow the jet evolution for a very long time even in the case of a high magnetic diffusivity (up to 4000 disk rotations). The observed de-collimation of the matter flow with increasing diffusivity is most evident if we plot the mass and momentum fluxes across the boundaries of the inner jet region.

In combination with various physical effects – magnetic and inertial forces, pressure and gravity – the magnetic diffusion will modify the MHD structure of the jet. As the flow approaches the Alfvén surface, a toroidal magnetic field component is induced (“wound-up”) due to the inertial back-reaction of the matter on the field. The toroidal field may lead to (de-) accelerating Lorentz forces

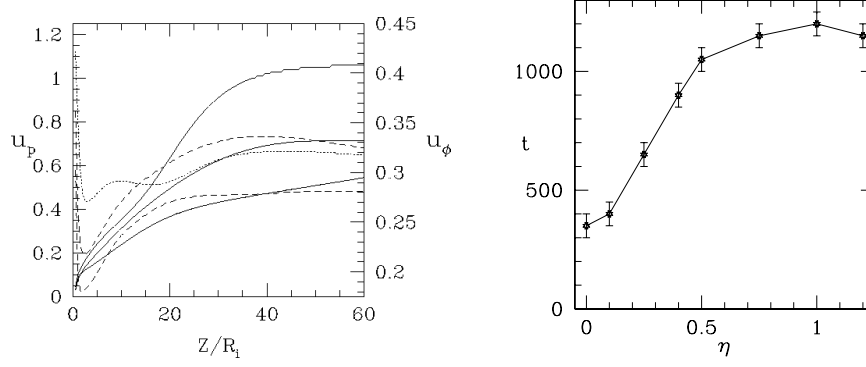


Figure 4: Left: Components of the velocities. Cuts in Z direction at  $r=15$  for the quasistationary time of simulations. Poloidal components are given in solid lines, toroidal in dashed lines. Two different ordinate scales are used to expose relative changes of the velocities. Left ordinate gives the values of the poloidal velocity, when right gives the values of the toroidal velocity. Both components increase with the increasing diffusivity. Right panel: The times when the quasistationary state is reached, in dependence on diffusivity.

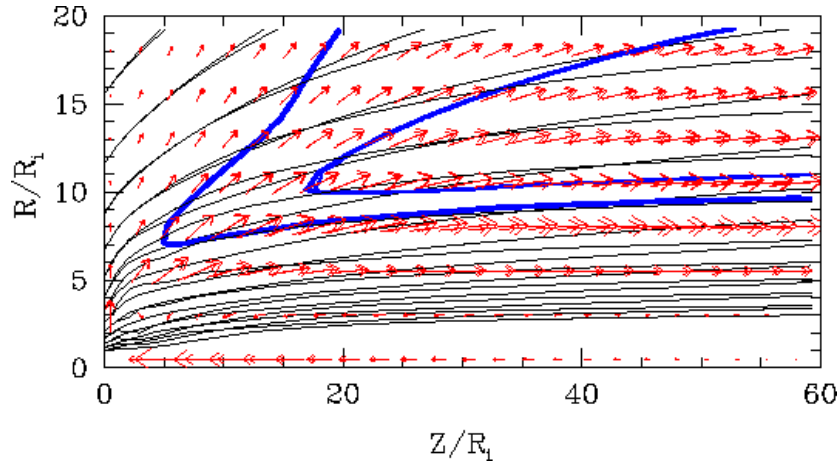


Figure 5: The de-collimation of the stationary state poloidal magnetic field due to magnetic diffusivity. Thick black lines for  $\eta=0$ , and thin lines for  $\eta=0.1$ . Overly of the poloidal velocity vectors show that the velocity pattern is not de-collimated. Thick blue line is the Alfvén surface, and thin blue line is the fast magnetosonic surface for the diffusive simulation.

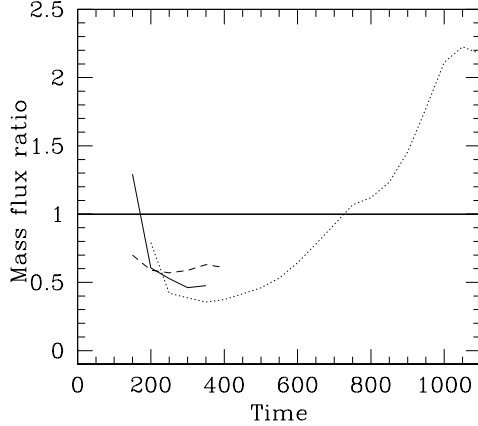


Figure 6: Time evolution of the mass flux ratio between the radial outflow boundary and the axial outflow boundary in the inner part of the jet,  $(z \times r) = (60 \times 20)r_i$ . Parameter  $\eta = 0, 0.1, 0.5$  in solid, dashed and dotted line, respectively. For higher diffusivity, the mass flux ratio in the quasi-stationary state increases, indicating a decrease in degree of collimation.

$\vec{F}_{L,\parallel} \sim \vec{j}_\perp \times \vec{B}_\phi$  and (de-) collimating forces  $\vec{F}_{L,\perp} \sim \vec{j}_\parallel \times \vec{B}$  where, here, the perpendicular and parallel projection is made with respect to the poloidal magnetic field (which, only in the case of ideal stationary MHD is parallel to the poloidal velocity).

The winding-up of the poloidal magnetic fields is less efficient since magnetic diffusion leads to a slip of matter across the field. The induced toroidal magnetic field is weaker leading to a less efficient acceleration by Lorentz forces but also to a de-collimation. As a de-collimation of the poloidal magnetic structure also implies a smaller launching angle for the sub-Alfvénic flow, the magneto-centrifugal acceleration mechanism may work more effective.

acknowledgements: We thank the LCA team and M. Norman for the possibility to use the ZEUS-3D code. This work was partly financed by the DFG Schwerpunktprogramm “Physik der Sternentstehung” (FE490/2-1).

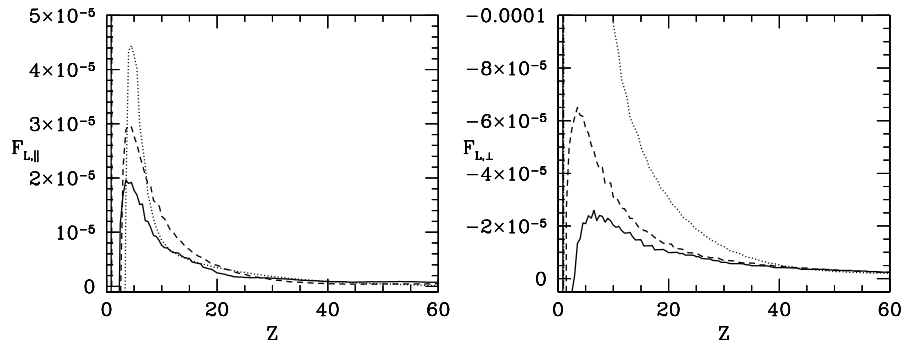


Figure 7: Lorentz forces in the jet for different magnetic diffusivity  $\eta = 0, 0.1, 0.5$  (solid, dashed and dotted lines, respectively). (Normalized) values of the force component perpendicular (left panel) and parallel (right panel) to the field line. The toroidal component is similar to the parallel one. Components are projected along a flux surface leaving the box of the inner jet close to  $(R=20, Z=60)$ -corner. The sign is defined as follows. For the perpendicular component the positive sign denotes the  $r$ -direction (de-collimating force). For the parallel component the positive sign denotes the  $z$ -direction (accelerating force).